



Mud removal and cement placement during primary cementing of an oil well

Laminar non-Newtonian displacements in an eccentric annular Hele-Shaw cell

S.H. BITTLESTON¹, J. FERGUSON¹ and I.A. FRIGAARD^{*,2}

¹Schlumberger Cambridge Research, High Cross, Madingley Road, Cambridge, CB3 0EL, England

²Department of Mathematics and Department of Mechanical Engineering, University of British Columbia, 2324 Main Mall, Vancouver, BC, V6T 1Z4 Canada; *Author for correspondence. (E-mail: frigaard@interchange.ubc.ca)

Received 11 June 2001; accepted in revised form 23 March 2002

Abstract. A two-dimensional model is derived of the displacement flows that occur during primary cementing of oil and gas wells. The displacement geometry is a long narrow eccentric annulus, between the casing and the rock formation. The model consists of a series of first-order convection equations for the fluid concentrations and a quasi-linear Poisson-type equation for the stream function. Coupling is through the velocity field and the concentration-dependent fluid properties.

A range of computed results from this model is presented. One simulation illustrates how a channel of mud can be left behind on the narrow side of the annulus. Another shows that stable steady-state displacements can occur, although conditions under which this occurs are not yet understood. A third simulation captures some of the complexity that occurs in realistic cementing operations.

Key words: displacement flows, Hele-Shaw cell, non-Newtonian fluids, visco-plastic fluid flow

1. Introduction

In this paper we consider laminar cementing displacement flows in narrow eccentric annuli, (an oil or gas well). As well as deriving a model that describes the bulk fluid motion, we present a number of examples that demonstrate the utility of this type of model for understanding practical cementing flows and improving displacements. The following coupled system of partial differential equations is derived and is the basis of our computational results.

$$\nabla_a \cdot \mathbf{S} = -f, \tag{1}$$

$$\frac{\partial}{\partial t} [Hr_a \bar{c}_k] + \frac{\partial}{\partial \phi} [H\bar{v} \bar{c}_k] + \frac{\partial}{\partial \xi} [Hr_a \bar{w} \bar{c}_k] = 0, \quad k = 1, 2, \dots, K, \tag{2}$$

$$\frac{\partial \Psi}{\partial \phi} = Hr_a \bar{w}, \quad \frac{\partial \Psi}{\partial \xi} = -H\bar{v}. \tag{3}$$

This is essentially a Hele-Shaw displacement model. The *unwrapped* narrow annular space is $(\phi, \xi) \in (0, 1) \times (0, Z)$, the annular gap half-width is $H(\phi, \xi)$, which varies eccentrically with ϕ . A sequence of K fluids is pumped around the wellbore, each with a concentration \bar{c}_k ; Ψ is the stream function, which is determined from (1) and the following visco-plastic constitutive laws:

$$S = \left[\frac{r_a \chi(|\nabla_a \Psi|)}{|\nabla_a \Psi|} + \frac{r_a \tau_Y}{H |\nabla_a \Psi|} \right] \nabla_a \Psi \iff |S| > \frac{r_a \tau_Y}{H}, \quad (4)$$

$$|\nabla_a \Psi| = 0 \iff |S| \leq \frac{r_a \tau_Y}{H}, \quad (5)$$

which are derived from the true constitutive laws of the fluids. In (1)–(5), f contains the buoyancy terms, r_a is the local mean radius of the annulus, χ is a positive increasing function of $|\nabla_a \Psi|$, arising from the viscous shear-thinning behaviour of the fluids, and τ_Y is the fluid yield stress. Aside from the complication of visco-plastic behaviour, (1) is essentially a quasi-linear Poisson-type equation for Ψ .

1.1. PROCESS DESCRIPTION

In constructing oil or gas wells it is necessary to cement a series of steel casings or liners into the well as the depth increases. These cemented steel tubes serve a dual purpose. First, the cemented casings serve to support the wellbore, preventing collapse. Second, the cement provides a hydraulic seal on the outside of the steel tubing. A hydraulic seal is necessary in order to isolate the different fluid-bearing zones of the rock formation from one another and from the surface. Failure to achieve proper zonal isolation can have a significant economic effect in terms of lost well productivity, [1], and can also have adverse environmental effects. The latter are not felt during the productive life of a well, but later at abandonment, when pressures in the cemented annulus at the surface of the well prevent the well from being completely abandoned. Such wells are either *suspended/shut-in* on a semi-permanent basis, or expensive remedial treatment is carried out. The environmental problem is becoming increasingly important to the oil industry as significant numbers of oil and gas wells with surface casing pressures are being identified, [2].

The primary cementing process proceeds as follows; see Figure 1. A new section of the well is drilled. The drillpipe is removed from the wellbore, leaving drilling mud inside the wellbore. A steel tube (casing or liner) is inserted into the wellbore, typically leaving a gap of $\approx 2\text{cm}$ between the outside of the tube and the inside of the wellbore, *i.e.* the annulus. The tubing is inserted in sections of length $\approx 10\text{m}$ each. At certain points, *centralizers* are fitted to the outside of the tube, to prevent the heavy steel tubing from slumping to the lower side of the wellbore. However, it is still very common that the annulus is eccentric, especially in inclined wellbores. Once the tube is in place, with drilling mud on the inside and outside, a sequence of fluids are circulated down the inside of the tubing reaching bottom-hole and returning up the outside of the annulus. Typically, a wash or spacer fluid is pumped first, followed by one or more cement slurries. The rheologies and densities of the spacer and cement slurries can be designed so as to aid in displacement of the annulus drilling mud, within the constraints of maintaining well security.¹ The fluid volumes are designed so that the cement slurries fill the annular space to be cemented. Drilling mud follows the final cement slurry to be pumped and the circulation is stopped with a few metres of cement at the bottom of the inside of the casing, see final figure in Figure 1, and the cement is allowed to set. The final part of cement inside the tubing is drilled out as the well proceeds.

With reference to Figure 1, it can be seen that the completed well often has a telescopic arrangement of casings and liners. A liner is a casing that extends downwards from just above the previous casing. The steel tubing is a significant part of the material cost of a primary cementing operation; hence the use of liners in the lower parts of the well. Additionally, each

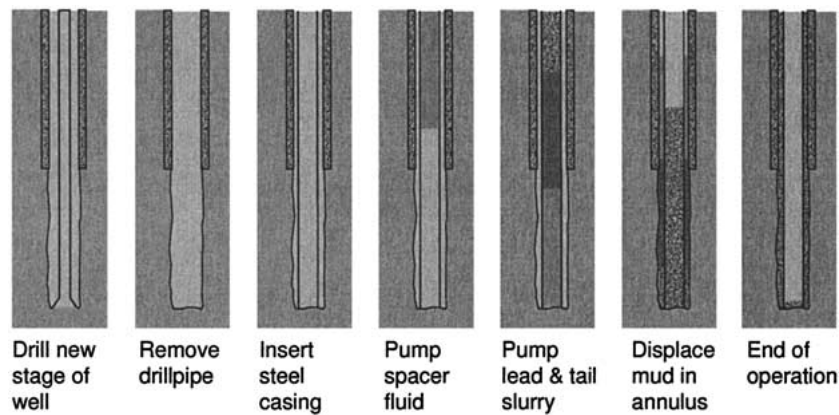


Figure 1. Schematic of the primary cementing process, showing the various stages (left to right) in cementing a new casing.

cement job is focused at zonal isolation of the exposed part of the wellbore. Thus, a cheaper cement slurry might be used to fill the part of the annulus inside the previous casing and/or this segment may be only partially filled. Typically, well inner diameters can start at anything up to $\sim 50\text{cm}$ and can end as small as $\sim 10\text{cm}$ in the producing zone. Extremes occur outside of these ranges and obviously diameters depend on the local conditions and intended length of the well. The cemented sections typically have lengths of order 300–1000m.

The means by which zonal isolation becomes impaired during cementing are various. Shrinkage/thermal stress effects during cement setting can combine to produce a range of mechanical defects allowing fluid pathways to form in the cement. Formation gases may enter the annulus as the cement sets and the static pressure drops, migrating upwards in the annulus. We do not study either of these interesting processes here. A reasonably up to date overview of current oilfield knowledge of these processes may be found in [3], which also contains further general process information. A final possible cause of impaired zonal isolation is that the mud is not fully removed from the annulus during the displacement process, remaining either on the annulus walls or in a channel filling the narrow side of the annulus. As the cement sets, water is removed from the mud leaving behind a porous conduit along which formation fluids can migrate. It is this possibility that is the focus for the work presented here.

Design methodologies for primary cementing that consider the rheology of the fluids have a long history. The possibility of a mud channel forming on the narrow side of the annulus was first identified in [4]. The reasoning used in [4] is essentially a hydraulic approach. Extensions have led to whole systems of design rules for laminar displacements, [5–9], also based on hydraulic reasoning. In general, these rule sets state that the flow rate must be sufficiently high to avoid a mud channel on the narrow side of the annulus, that there should be a hierarchy of the fluid rheologies pumped, (*i.e.* each fluid should generate a higher frictional pressure than its predecessor), and that there should be a hierarchy of the fluid densities, (each fluid heavier than its predecessor). Successful applications of such rule-based systems, typically implemented with a one-dimensional hydraulics-type computer simulation, are given in . Whilst such approaches obviously contain a number of physical truths, the level of fundamental understanding is low and predictions made are generally conservative. A further problem with such systems is in making predictions for highly deviated and horizontal wellbores. Amongst the difficulties here, positive density differences, which help displacement in

near vertical wells, tend to cause slumping towards the lower side of the annulus in highly deviated sections, see [13–15].

Putting aside the industrial motivation, more fundamental and detailed approaches have focused on computing the entire annular flow. However, this work is relatively recent. The first reliable analyses of narrow eccentric annular flows of visco-plastic fluids were carried out in the early 1990's, see [16, 17], and this only for flows of a single fluid in 2 spatial dimensions. Three-dimensional Newtonian displacements in eccentric annular geometries have been computed in [18, 19], but a fully three-dimensional approach is obviously restrictive when it comes to designing displacements over the scale of the wellbore. Here instead, we attempt to isolate the different phenomena present in the wellbore during displacement and study each separately.

In [20–23] we have considered displacements in long axial ducts, *i.e.* two-dimensional slots and axisymmetric flows in pipes. The two-dimensional geometry allows some simplification and significant progress has been made in understanding the processes by which a static layer of mud can be left on the walls of the annulus, theoretically, numerically and experimentally. For symmetric iso-density displacements, it is possible to predict reasonably well the thickness of residual mud layers, [20, 22, 23], but for inclined and buoyant displacements the same problem has so far eluded a simple solution, [24, pp. 55–62]. Here we consider the complementary problem of studying the bulk fluid movements in the annulus. The genesis of this approach is in [25] and a simplified version of the model that we derive here has been validated against a series of experiments in [26, 27].

The aim of our model is to be able to analyse process features that are evidently related to the large-scale/bulk fluid motions occurring during displacement. For example, if the annulus is very eccentric or if the mud has a very large yield stress, it is simply not displaced on the narrow side of the annulus. This is clearly not an interfacial phenomenon. Similarly, if the fluid properties are well designed, it is possible that the drilling mud is displaced in a stable steady interface. We would like to understand both types of phenomena, and others, as well as being able to simulate realistic displacements flows that occur in wells, where the full complexity of changing annular geometries, diverse fluid properties and fluctuating flow rates, is found.

In considering bulk fluid motions by averaging across the annular duct, we are inevitably drawn towards analogies with classical Hele-Shaw displacement studies; see [28] and the reviews [29, 30]. Although the analogy clearly exists, we do not wish to emphasise it. Our work is directed at the cementing process and we wish to extract the results of most practical relevance to this process. In particular, the majority of investigations in this area focus specifically on the study of fingering instabilities (by whatever mechanism). On the other hand in cementing it is industry practice to try to avoid such instabilities, *e.g.* by using a heavier and more viscous fluid to displace with wherever feasible. This does not deny the existence of such instabilities in cementing, but their detailed study requires more effort than can be devoted here. In the context of a porous media flow our displacements are through an anisotropic spatially varying media, due to the eccentricity of the annulus. A second complication is that our displacements involve non-Newtonian fluids. Although there have been many studies of classical Hele-Shaw displacements with non-Newtonian fluids, *e.g.* starting with [31], general conclusions have not been drawn. Indeed, for the Herschel-Bulkley fluids that we consider, it is only very recently that the question of modelling classical Hele-Shaw fingering displacements has been tackled, [32], (but see also the earlier and closely related work of [33–35]). A third difference in our work, compared to many Hele-Shaw displacements, is that we consider miscible displacements although our eventual model contains only passive

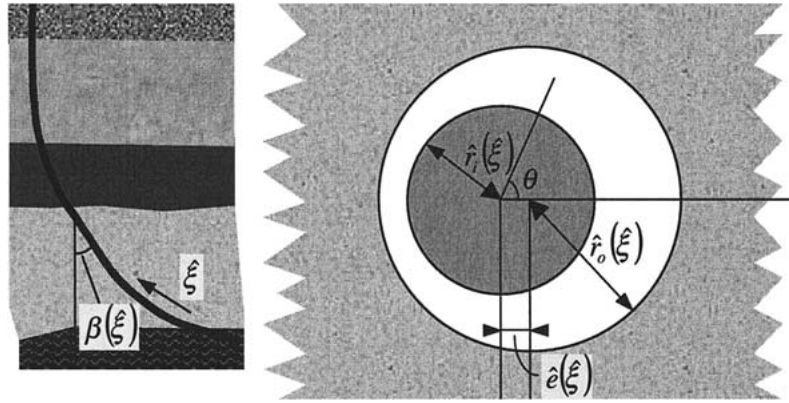


Figure 2. Schematic of the well and of the variables that describe the eccentric annular geometry in a cross-section

scalar advection, (*i.e.* although miscible they do not mix on these timescales). This (routine) treatment of miscible displacements has been studied in some depth, *e.g.* [36, 37], and can be questionable in the case of unstable displacements. This is one of many areas for future investigation. Finally, we remark that it is only fairly recently that it has been shown that surface tension is not necessary to produce exact time-dependent fingering solutions without singularities, [38].

1.2. OUTLINE

An outline of the paper is as follows. In Section 2 we use classical dimensional scaling methods to reduce the full three-dimensional equations of motion. The modelling process is completed in Section 3, wherein Equations (1)–(3) are derived. Section 4 presents numerical simulation results from a simplified version of (1)–(3). The paper ends with a brief discussion.

2. Modelling bulk displacement flows

A cylindrical coordinate system $(\hat{r}, \theta, \hat{\xi})$ is used to describe the well geometry; $\hat{\xi}$ measures distance along the central axis of the casing $\hat{r} = 0$, (*i.e.* $\hat{\xi}$ is the *measured depth*, but measured upwards from bottom-hole). Wells are typically inclined to the vertical and the inclination angle is denoted $\beta(\hat{\xi})$. The local cross-section of the well, outside the casing, is assumed to be that of an eccentric annulus, with inner radius $\hat{r}_i(\hat{\xi})$, equal to the outer radius of the casing and outer radius $\hat{r}_o(\hat{\xi})$ equal to the inner radius of the hole (or previous casing). At each depth $\hat{\xi}$, the mean radius $\hat{r}_a(\hat{\xi})$ and the mean half-gap width $\hat{d}(\hat{\xi})$ are defined by:

$$\hat{r}_a(\hat{\xi}) \equiv \frac{1}{2}[\hat{r}_o(\hat{\xi}) + \hat{r}_i(\hat{\xi})], \quad \hat{d}(\hat{\xi}) \equiv \frac{1}{2}[\hat{r}_o(\hat{\xi}) - \hat{r}_i(\hat{\xi})]. \quad (6)$$

As well as inner and outer radii the displacement, $\hat{e}(\hat{\xi})$, of the two centres of the two cylinders is given, see Figure 2. The following three geometrical assumptions are made: (i) that the cylinders do not touch, ($\hat{e}(\hat{\xi}) < 2\hat{d}(\hat{\xi})$); (ii) all variations in the cross-section geometry and inclination, axially along the wellbore, are *slow*; (iii) the weight of the casing acts in such a way that the narrow side of the annulus will be found on the lower side of the well.

The annular displacement is modelled as a concentration dependent multi-fluid flow that is both laminar and incompressible.² In the local coordinate system:

$$\hat{\rho} \left[\frac{\partial}{\partial \hat{t}} + \hat{\mathbf{u}} \cdot \hat{\nabla} \right] \hat{u} = \frac{1}{\hat{r}} \frac{\partial}{\partial \hat{r}} [\hat{r} \hat{\tau}_{\hat{r}\hat{r}}] + \frac{1}{\hat{r}} \frac{\partial}{\partial \theta} \hat{\tau}_{\hat{r}\theta} + \frac{\partial}{\partial \hat{\xi}} \hat{\tau}_{\hat{r}\hat{\xi}} - \frac{\hat{\tau}_{\theta\theta}}{\hat{r}} - \frac{\partial \hat{p}}{\partial \hat{r}} + \hat{\rho} \hat{g}_{\hat{r}}, \quad (7)$$

$$\hat{\rho} \left[\frac{\partial}{\partial \hat{t}} + \hat{\mathbf{u}} \cdot \hat{\nabla} \right] \hat{v} = \frac{1}{\hat{r}^2} \frac{\partial}{\partial \hat{r}} [\hat{r}^2 \hat{\tau}_{\theta\hat{r}}] + \frac{1}{\hat{r}} \frac{\partial}{\partial \theta} \hat{\tau}_{\theta\theta} + \frac{\partial}{\partial \hat{\xi}} \hat{\tau}_{\theta\hat{\xi}} - \frac{1}{\hat{r}} \frac{\partial \hat{p}}{\partial \theta} + \hat{\rho} \hat{g}_{\theta}, \quad (8)$$

$$\hat{\rho} \left[\frac{\partial}{\partial \hat{t}} + \hat{\mathbf{u}} \cdot \hat{\nabla} \right] \hat{w} = \frac{1}{\hat{r}} \frac{\partial}{\partial \hat{r}} [\hat{r} \hat{\tau}_{\hat{\xi}\hat{r}}] + \frac{1}{\hat{r}} \frac{\partial}{\partial \theta} \hat{\tau}_{\hat{\xi}\theta} + \frac{\partial}{\partial \hat{\xi}} \hat{\tau}_{\hat{\xi}\hat{\xi}} - \frac{\partial \hat{p}}{\partial \hat{\xi}} + \hat{\rho} \hat{g}_{\hat{\xi}}, \quad (9)$$

$$0 = \frac{1}{\hat{r}} \frac{\partial}{\partial \hat{r}} [\hat{r} \hat{u}] + \frac{1}{\hat{r}} \frac{\partial \hat{v}}{\partial \theta} + \frac{\partial \hat{w}}{\partial \hat{\xi}}, \quad (10)$$

where $\hat{\mathbf{u}} = (\hat{u}, \hat{v}, \hat{w})$ is the velocity, and \hat{p} is the pressure. Components of the deviatoric stress are denoted $\hat{\tau}_{ij}$. We assume that a sequence of K fluids is pumped around the flow path. Each fluid and any resulting mixture is assumed to be adequately described as an inelastic generalised non-Newtonian fluid.³ We specify constitutive laws later. In (7)–(9), the vector of gravitational accelerations, $\hat{\mathbf{g}} = (\hat{g}_{\hat{r}}, \hat{g}_{\theta}, \hat{g}_{\hat{\xi}})$, is given by

$$\hat{g}_{\hat{r}} = \hat{g} \sin \beta(\hat{\xi}) \cos \theta, \quad \hat{g}_{\theta} = \hat{g} \sin \beta(\hat{\xi}) \sin \theta, \quad \hat{g}_{\hat{\xi}} = \hat{g} \cos \beta(\hat{\xi}), \quad (11)$$

where $\hat{g} = 9.81 \text{m/s}^2$. The concentrations of each individual fluid component c_k are modeled by an advection-diffusion equation:

$$\frac{\partial c_k}{\partial \hat{t}} + \frac{1}{\hat{r}} \frac{\partial}{\partial \hat{r}} [\hat{r} \hat{u} c_k] + \frac{1}{\hat{r}} \frac{\partial}{\partial \theta} [\hat{v} c_k] + \frac{\partial}{\partial \hat{\xi}} [\hat{w} c_k] = \hat{\nabla} \cdot [\hat{D}_k(\mathbf{c}, \hat{\mathbf{u}}) \hat{\nabla} c_k], \quad (12)$$

where $\sum_{k=1}^K c_k = 1$. The density and the rheological parameters of the fluids are assumed to depend upon the concentrations of fluids present, *e.g.* $\hat{\rho} = \hat{\rho}(\mathbf{c})$, where $\mathbf{c} = (c_1, c_2, \dots, c_K)$.

2.1. NON-DIMENSIONALISATION

We reduce our model to something more tractable than the above system (7)–(10) and (12), by averaging across the gap thickness and by using standard scaling arguments. The annulus geometry is long and thin, with the typical gap half-width ($\sim 1\text{cm}$) being much smaller than a typical azimuthal distance ($\sim 30\text{cm}$), which in turn is much smaller than a typical length of the annulus ($\sim 500\text{m}$). Our intention is to derive a two-dimensional model of the bulk fluid motions, in azimuthal and axial directions. We thus focus on eliminating the radial dependency.

2.1.1. Geometry and velocity scales

Denote the total length of the zone of the well to be cemented by \hat{Z} . It is assumed that this zone extends upwards from bottom hole, $\hat{\xi}_{bh}$, to the top of the zone, $\hat{\xi}_{tz}$, *i.e.* $\hat{Z} = \hat{\xi}_{tz} - \hat{\xi}_{bh}$. The mean radius \hat{r}_a^* is:

$$\hat{r}_a^* = \frac{1}{\hat{Z}} \int_{\hat{\xi}_{bh}}^{\hat{\xi}_{tz}} \hat{r}_a(\hat{\xi}) d\hat{\xi}. \quad (13)$$

Scaled axial and azimuthal coordinates ξ and ϕ are then:

$$\xi = \frac{\hat{\xi} - \hat{\xi}_{bh}}{\pi \hat{r}_a^*}, \quad \phi = \frac{\theta}{\pi}. \quad (14)$$

Local and global measures of the narrowness of the annulus, $\delta(\hat{\xi})$ and δ^* , respectively, are defined by:

$$\delta(\hat{\xi}) = \frac{\hat{d}(\hat{\xi})}{\hat{r}_a(\hat{\xi})}, \quad \delta^* = \frac{1}{\hat{Z}} \int_{\hat{\xi}_{bh}}^{\hat{\xi}_{tz}} \delta(\hat{\xi}) \, d\hat{\xi}. \quad (15)$$

We will rely on the smallness of the parameter δ^*/π , which denotes the ratio of radial to azimuthal length-scales, in order to reduce our system. In each cross-section, we define the local average radius, $r = r_a(\xi)$, and local annulus eccentricity, $e(\xi)$, by:

$$r_a(\xi) = \frac{\hat{r}_a(\hat{\xi})}{\hat{r}_a^*}, \quad e(\xi) = \frac{\hat{e}(\hat{\xi})}{2\hat{d}(\hat{\xi})}. \quad (16)$$

The centreline of the annular gap is at $\hat{r} = \hat{r}_a^* r_a(\xi) r_c(\phi, \xi)$. Inner and outer walls have radial positions, $\hat{r} = \hat{r}_a^* r_a(\xi) [r_c(\phi, \xi) \mp \delta(\xi) h(\phi, \xi)]$. For small $\delta(\xi)$, the following expressions define $r_c(\phi, \xi)$ and $h(\phi, \xi)$:

$$r_c(\phi, \xi) \sim 1 + e(\xi)\delta(\xi) \cos \pi\phi + [e(\xi)\delta(\xi) \sin \pi\phi]^2 + O(\delta^3), \quad (17)$$

$$h(\phi, \xi) \sim 1 + e(\xi) \cos \pi\phi - [e(\xi)]^2 \delta(\xi) \sin \pi\phi + [e(\xi)\delta(\xi) \sin \pi\phi]^2 + O(\delta^3). \quad (18)$$

The approximation that we use assumes both narrowness and uniformity of the annular geometry in the sense that $\delta(\xi) \sim \delta^* \ll 1$, by setting:

$$r_c(\phi, \xi) = 1, \quad h(\phi, \xi) = 1 + e(\xi) \cos \pi\phi. \quad (19)$$

The radial coordinate is scaled relative to the distance from the centreline of the annulus, as follows:

$$y = \frac{\hat{r} - \hat{r}_a^* r_a(\xi) r_c(\phi, \xi)}{\hat{r}_a^* \delta^*}, \quad (20)$$

i.e. y is a local annular gap coordinate. The inner and outer walls are given to leading order by $y = \mp H(\phi, \xi)$, where:

$$H(\phi, \xi) = \frac{\delta(\xi) r_a(\xi) [1 + e(\xi) \cos \pi\phi]}{\delta^*}. \quad (21)$$

To scale the fluid velocities we first define a typical cross-sectional area of the annulus: $\hat{A}^* = 4\pi \delta^* [\hat{r}_a^*]^2$. Secondly, we define a scale \hat{Q}^* for the flow rates via

$$\hat{Q}^* = \max_{\hat{t}} \hat{Q}_{\text{pump}}(\hat{t}), \quad (22)$$

where $\hat{Q}_{\text{pump}}(\hat{t})$ is the pump schedule, typically a step function. The dimensionless flow rate is then simply

$$Q(t) = \frac{\hat{Q}(\hat{t})}{\hat{Q}^*}. \quad (23)$$

All axial and azimuthal velocities are scaled with \hat{w}^* , defined straightforwardly by:

$$\hat{w}^* = \frac{\hat{Q}^*}{\hat{A}^*}, \quad (24)$$

and radial velocities are scaled with $\hat{w}^* \delta^* / \pi$. A dimensionless time is defined from the axial length and velocity scales by:

$$\hat{t} = \hat{t}^* t, \quad \hat{t}^* = \frac{\pi \hat{r}_a^*}{\hat{w}^*}. \quad (25)$$

2.1.2. Fluid description, stress and fluid property scaling

We assume that each fluid k can be described as an Herschel-Bulkley fluid, characterised by a vector $(\hat{\rho}_k, \hat{\tau}_{k,Y}, \hat{\kappa}_k, n_k)$, denoting the density, yield stress, consistency and power-law index, respectively. A characteristic scale for the rate of strain is $\hat{\gamma}^*$:

$$\hat{\gamma}^* = \frac{\hat{w}^*}{\hat{r}_a^* \delta^*}, \quad (26)$$

and this is used to define scales for the shear stress, viscosity and pressure, as follows:

$$\hat{\tau}^* = \max_k [\hat{\tau}_{k,Y} + \hat{\kappa}_k (\hat{\gamma}^*)^{n_k}], \quad \hat{\mu}^* = \frac{\hat{\tau}^*}{\hat{\gamma}^*}, \quad \hat{p}^* = \frac{\hat{\tau}^* \pi}{\delta^*}. \quad (27)$$

All shear stress components are scaled with $\hat{\tau}^*$ and dimensional rheological parameters are defined by:

$$\hat{\tau}_{k,Y} = \hat{\tau}^* \tau_{k,Y}, \quad \hat{\kappa}_k (\hat{\gamma}^*)^{n_k-1} = \hat{\mu}^* \kappa_k, \quad n_k = n_k. \quad (28)$$

The fluid densities are scaled with $\hat{\rho}^*$:

$$\hat{\rho}^* = \max_k [\hat{\rho}_k]. \quad (29)$$

2.2. SCALED SYSTEM OF EQUATIONS

With the scaling above, dimensionless field equations follow straightforwardly. Neglecting all terms of $O(\frac{\delta^*}{\pi})$, we arrive at:⁴

$$0 = -\frac{\partial p}{\partial y}, \quad (30)$$

$$0 = -\frac{1}{r_a} \frac{\partial p}{\partial \phi} + \frac{\partial}{\partial y} \tau_{\phi y} + \frac{\rho \sin \beta \sin \pi \phi}{St^*}, \quad (31)$$

$$0 = -\frac{\partial p}{\partial \xi} + \frac{\partial}{\partial y} \tau_{\xi y} - \frac{\rho \cos \beta}{St^*}. \quad (32)$$

The parameter St^* in (31) and (32) is a Stokes number for the displacement flow:

$$St^* = \frac{\hat{\mu}^* \hat{w}^*}{\hat{\rho}^* \hat{g}^* [\hat{r}_a^* \delta^*]^2} = \frac{\hat{\tau}^*}{\hat{\rho}^* \hat{g}^* \hat{r}_a^* \delta^*}. \quad (33)$$

The leading-order momentum equations (31) and (32) describe a bi-directional shear flow through a slot of width $2H(\phi, \xi)$, oriented in the (ϕ, ξ) -plane. The leading-order rates of strain are the terms involving y -derivatives of v and w , *i.e.* in regions where the fluid is yielded:

$$\tau_{\phi y} \sim \eta \frac{\partial v}{\partial y} + O\left(\frac{\delta^*}{\pi}\right), \quad \tau_{\xi y} \sim \eta \frac{\partial w}{\partial y} + O\left(\frac{\delta^*}{\pi}\right)$$

where η is an effective viscosity, which depends on the rate of strain invariant, $\dot{\gamma}$:

$$\dot{\gamma} \sim \left[\left(\frac{\partial v}{\partial y}\right)^2 + \left(\frac{\partial w}{\partial y}\right)^2 \right]^{1/2} + O\left(\frac{\delta^*}{\pi}\right).$$

Thus, to leading order the constitutive laws will depend only on the y -derivatives of both v and w , (and the local fluid concentrations).

This suggests that we can achieve closure by considering motion only in the (ϕ, ξ) -plane. To proceed in this direction we make two key assumptions.⁵ First, we assume that the fluid concentrations are homogeneous across the annular gap. Second, we assume that the velocity field (v, w) is approximated to within $O(\delta^*/\pi)$ by the corresponding symmetric *slot* velocity field, $s = (v_s, w_s)$, *i.e.* symmetric about the slot center $y = 0$.

With these assumptions, $p = p(\phi, \xi, t)$ and, in yielded regions of the flow, our leading order momentum equations are:

$$\frac{\partial}{\partial y} \left[\eta \frac{\partial v_s}{\partial y} \right] = \frac{1}{r_a} \frac{\partial p}{\partial \phi} - \frac{\rho \sin \beta \sin \pi \phi}{St^*}, \quad (34)$$

$$\frac{\partial}{\partial y} \left[\eta \frac{\partial w_s}{\partial y} \right] = \frac{\partial p}{\partial \xi} + \frac{\rho \cos \beta}{St^*}. \quad (35)$$

Neglecting terms of $O(\frac{\delta^*}{\pi})$, the scaled mass-conservation equation is:

$$\frac{\partial u}{\partial y} + \frac{1}{r_a} \frac{\partial v_s}{\partial \phi} + \frac{\partial w_s}{\partial \xi} = 0. \quad (36)$$

To eliminate u we average across the gap width, using conditions of no-slip at the annulus walls:

$$\frac{\partial}{\partial \phi} [H\bar{v}] + \frac{\partial}{\partial \xi} [r_a H\bar{w}] = 0, \quad (37)$$

where

$$\bar{v}(\phi, \xi, t) = \frac{1}{H} \int_0^H v_s \, dy, \quad \bar{w}(\phi, \xi, t) = \frac{1}{H} \int_0^H w_s \, dy, \quad (38)$$

recall that (v_s, w_s) are symmetric about $y = 0$. Equation (37) is satisfied using a stream function:

$$r_a H\bar{w} = \frac{\partial \Psi}{\partial \phi}, \quad H\bar{v} = -\frac{\partial \Psi}{\partial \xi}. \quad (39)$$

For the species concentration equations, we proceed analogously. We integrate across the local gap width, using the conditions of no-slip at the walls and the assumption that there is zero flux of any fluid across the walls. We have already assumed that there is no concentration gradient across the annulus gap. This assumption allows us to write the average of products of other variables with the concentrations, as products of averages. A weaker, but adequate, assumption here is to assume an $O(\delta^*/\pi)$ difference between the averages of the products and the products of the averages, on left-hand side of (12). Our reduced and scaled form of (12) is:

$$\frac{\partial}{\partial t} [Hr_a \bar{c}_k] + \frac{\partial}{\partial \phi} [H\bar{v} \bar{c}_k] + \frac{\partial}{\partial \xi} [Hr_a \bar{w} \bar{c}_k] = \frac{1}{\text{Pe}^*} \left(\frac{\partial}{\partial \phi} \left[\frac{H\bar{D}_k}{r_a} \frac{\partial \bar{c}_k}{\partial \phi} \right] + \frac{\partial}{\partial \xi} \left[Hr_a \bar{D}_k \frac{\partial \bar{c}_k}{\partial \xi} \right] \right). \tag{40}$$

The diffusivities have been scaled with a global diffusivity scale, say \hat{D}^* , and the Peclet number Pe^* is defined as

$$\text{Pe}^* = \frac{\pi \hat{r}_a^* \hat{w}^*}{\hat{D}^*}. \tag{41}$$

Considering the axial length of the cemented region of a well, we typically have $Z \sim 10^2 - 10^3$. Thus, at the end of pumping a job, (at mean speeds of size unity), we would typically have a diffuse layer of thickness $\sim \sqrt{Z/\text{Pe}^*}$. Typical sizes for $\pi \hat{r}_a^* \hat{w}^*$ are in the range $2 \times 10^{-2} - 5 \times 10^{-1} \text{m}^2 \text{s}^{-1}$. Therefore, provided that $\hat{D}^* \sim 10^{-6} \text{m}^2 \text{s}^{-1}$, the diffuse layer is negligible. Molecular diffusion in laminar flows is characterised by values $\hat{D}^* \sim 10^{-12} \text{m}^2 \text{s}^{-1}$, but other diffusive and dispersive processes might also be active here. We assume that the net effect of these processes results in a diffusive effect of size $\hat{D}^* \sim 10^{-6} \text{m}^2 \text{s}^{-1}$, or smaller.⁶ Our final model for the fluid concentrations is therefore:

$$\frac{\partial}{\partial t} [Hr_a \bar{c}_k] + \frac{\partial}{\partial \phi} [H\bar{v} \bar{c}_k] + \frac{\partial}{\partial \xi} [Hr_a \bar{w} \bar{c}_k] = 0, \tag{42}$$

where \bar{c}_k denotes the gap-averaged fluid concentration.

2.2.1. Constitutive laws

By assumption, the fluid concentrations do not vary across the width of the annular gap. Thus, in (34) and (35) the y -variation in η depends only on the leading-order rate of strain:

$$\dot{\gamma} = \left(\left[\frac{\partial v_s}{\partial y} \right]^2 + \left[\frac{\partial w_s}{\partial y} \right]^2 \right)^{1/2}. \tag{43}$$

We have assumed that each fluid is characterised as a Herschel-Bulkley fluid. A mixture model is used locally, to provide closure expression for the fluid properties in terms of the gap-averaged fluid concentrations:

$$\begin{aligned} \tau_Y(\bar{\mathbf{c}}) &= \sum_k \bar{c}_k \tau_{k,Y}, & \kappa(\bar{\mathbf{c}}) &= \sum_k \bar{c}_k \kappa_k, \\ n(\bar{\mathbf{c}}) &= \sum_k \bar{c}_k n_k, & \rho(\bar{\mathbf{c}}) &= \sum_k \bar{c}_k \rho_k. \end{aligned}$$

Apart from the density, the above *mixture* laws are used for simplicity, with no particular physical justification. In practice certain combinations of the fluids that are used in cementing are fully miscible, whereas others are wholly incompatible. It is therefore impossible to give a general description or model, without considerable further study.

Our reduced constitutive laws are:

$$\tau_{\phi y} = \left[\kappa(\bar{\mathbf{c}}) \dot{\gamma}^{(n(\bar{\mathbf{c}})-1)} + \frac{\tau_Y(\bar{\mathbf{c}})}{\dot{\gamma}} \right] \frac{\partial v_s}{\partial y} \iff [\tau_{\phi y}^2 + \tau_{\xi y}^2]^{1/2} > \tau_Y(\bar{\mathbf{c}}) \tag{44}$$

$$\tau_{\xi y} = \left[\kappa(\bar{c}) \dot{\gamma}^{(n(\bar{c})-1)} + \frac{\tau_Y(\bar{c})}{\dot{\gamma}} \right] \frac{\partial w_s}{\partial y} \iff [\tau_{\phi y}^2 + \tau_{\xi y}^2]^{1/2} > \tau_Y(\bar{c}) \quad (45)$$

$$\dot{\gamma} = 0 \iff [\tau_{\phi y}^2 + \tau_{\xi y}^2]^{1/2} \leq \tau_Y(\bar{c}). \quad (46)$$

In regions where the fluid is yielded, the effective viscosity η is:

$$\eta = \eta(\bar{c}, \dot{\gamma}) = \kappa(\bar{c}) \dot{\gamma}^{(n(\bar{c})-1)} + \frac{\tau_Y(\bar{c})}{\dot{\gamma}}. \quad (47)$$

3. Eccentric annular Hele-Shaw displacement model

By integrating (34) and (35) three times with respect to y , we arrive at:⁷

$$\bar{v} = - \left[\frac{1}{r_a} \frac{\partial p}{\partial \phi} - \frac{\rho \sin \beta \sin \pi \phi}{St^*} \right] \frac{1}{H} \int_0^H \int_y^H \frac{\tilde{y}}{\eta(\tilde{y})} d\tilde{y} dy, \quad (48)$$

$$\bar{w} = - \left[\frac{\partial p}{\partial \xi} + \frac{\rho \cos \beta}{St^*} \right] \frac{1}{H} \int_0^H \int_y^H \frac{\tilde{y}}{\eta(\tilde{y})} d\tilde{y} dy, \quad (49)$$

where the integrand on the right-hand side is zero in an unyielded region of the flow, *i.e.* $\eta \rightarrow \infty$ and $\dot{\gamma} \rightarrow 0$ in such regions. It follows that the vector of averaged velocities (\bar{v}, \bar{w}) is parallel in the (ϕ, ξ) plane to the vector \mathbf{G} :

$$\mathbf{G} = (G_\phi, G_\xi) \equiv \left(-\frac{1}{r_a} \frac{\partial p}{\partial \phi} + \frac{\rho \sin \beta \sin \pi \phi}{St^*}, -\frac{\partial p}{\partial \xi} - \frac{\rho \cos \beta}{St^*} \right), \quad (50)$$

which is the vector of modified pressure gradients.

We write G for the absolute value of the modified pressure gradient, *i.e.* $G = [G_\phi^2 + G_\xi^2]^{1/2}$. In a local coordinate direction that is aligned to the direction of the gap-averaged flow, the velocity is denoted s and the momentum equations (34) and (35) become simply:

$$\frac{\partial}{\partial y} \tau = -G, \quad (51)$$

where

$$\tau = \eta(\bar{c}, \left| \frac{\partial s}{\partial y} \right|) \frac{\partial s}{\partial y} \iff |\tau| > \tau_Y, \quad \left| \frac{\partial s}{\partial y} \right| = 0 \iff |\tau| \leq \tau_Y, \quad (52)$$

i.e. if the coordinate direction is correctly chosen, the flow is simply a Poiseuille flow between two (locally) parallel plates. By integrating (51) with respect to y , using the conditions of symmetry ($\tau = 0$) at $y = 0$ and no-slip ($s = 0$) at $y = H$, we find the closure relationship between G and the slot-averaged speed $|\bar{s}| \equiv [\bar{v}^2 + \bar{w}^2]^{1/2}$. This relationship is essentially the relationship between pressure drop and flow rate for a Poiseuille flow through a plane channel, which we write as: $H|\bar{s}| = F(G)$. In terms of our variables, the function $F(G)$ is:

$$F(G) = \begin{cases} 0 & HG \leq \tau_Y, \\ \frac{(HG - \tau_Y)([m+1]HG + \tau_Y)}{G^2(m+1)(m+2)} \left[\frac{HG - \tau_Y}{\kappa} \right]^m & HG > \tau_Y, \end{cases} \quad (53)$$

where $n = 1/m$.

We are now in a position to significantly simplify our model. First we introduce azimuthal gradient and divergence operators, ∇_a and $\nabla_a \cdot$:

$$\nabla_a q = \left(\frac{1}{r_a(\xi)} \frac{\partial q}{\partial \phi}, \frac{\partial q}{\partial \xi} \right), \quad \nabla_a \cdot \mathbf{q} = \frac{1}{r_a(\xi)} \frac{\partial q_\phi}{\partial \phi} + \frac{\partial q_\xi}{\partial \xi},$$

for arbitrary q and $\mathbf{q} = (q_\phi, q_\xi)$. We note that $H|\bar{\nu}| \equiv |\nabla_a \Psi|$, and that (53) is effectively a closure law of form:

$$|\nabla_a \Psi| = F(G). \quad (54)$$

It is evident from (53) that where GH does not exceed τ_Y there will be no flow, $|\nabla_a \Psi| = 0$. Suppose therefore that $|\nabla_a \Psi| \neq 0$. Equations (48) and (49) imply that:

$$\frac{\frac{\partial \Psi}{\partial \xi}}{|\nabla_a \Psi|} = \frac{G_\phi}{G}, \quad \frac{\frac{1}{r_a(\xi)} \frac{\partial \Psi}{\partial \phi}}{|\nabla_a \Psi|} = \frac{G_\xi}{G}. \quad (55)$$

We can convert the system (55) into a field equation for either the pressure field or the stream function. The pressure field is, however, indeterminate in regions of the flow where $|\nabla_a \Psi| = 0$. Thus, we select the stream function as our base variable.

We assume that $H > 0$ and that our fluids satisfy $\kappa > 0$ and $m \geq 1$, *i.e.* they are shear-thinning viscous fluids; we allow both $\tau_Y = 0$ and $\tau_Y > 0$. We rearrange (53) by defining χ by:

$$\chi = G - \frac{\tau_Y}{H}, \quad (56)$$

and then we have

$$|\nabla_a \Psi| = \begin{cases} 0 & \chi \leq 0, \\ \frac{H^{m+2}}{\kappa^m(m+2)} \frac{\chi^{m+1}}{(\chi + \tau_Y/H)^2} \left[\chi + \frac{(m+2)\tau_Y}{(m+1)H} \right] & \chi > 0. \end{cases} \quad (57)$$

The relationship between $|\nabla_a \Psi| \geq 0$ and $\chi \geq 0$, given by (57) is continuous and monotone, and therefore can be inverted, albeit numerically. Writing therefore $\chi = \chi(|\nabla_a \Psi|)$ to denote the function defined by inverting (57), we have that:

$$G = F^{-1}(|\nabla_a \Psi|) = \chi(|\nabla_a \Psi|) + \frac{\tau_Y}{H}, \quad (58)$$

if $|\nabla_a \Psi| > 0$, and G is undetermined elsewhere. Rearranging (55) and substituting for G , we have

$$-r_a G_\phi = \frac{\partial p}{\partial \phi} - \frac{r_a \rho \sin \beta \sin \pi \phi}{St^*} = \frac{r_a(\chi(|\nabla_a \Psi|) + \tau_Y/H)}{|\nabla_a \Psi|} \frac{\partial \Psi}{\partial \xi} \quad (59)$$

$$G_\xi = -\frac{\partial p}{\partial \xi} - \frac{\rho \cos \beta}{St^*} = \frac{\chi(|\nabla_a \Psi|) + \tau_Y/H}{|\nabla_a \Psi|} \frac{1}{r_a} \frac{\partial \Psi}{\partial \phi}. \quad (60)$$

Cross-differentiating to eliminate the pressure, leads to:

$$\nabla_a \cdot \left[\frac{r_a(\chi(|\nabla_a \Psi|) + \tau_Y/H)}{|\nabla_a \Psi|} \nabla_a \Psi \right] = -f, \quad (61)$$

where f is given by:

$$f = \nabla_a \cdot \left(\frac{r_a \rho(\bar{c}) \cos \beta}{St^*}, \frac{r_a \rho(\bar{c}) \sin \beta \sin \pi \phi}{St^*} \right). \quad (62)$$

Equation (61) is formally defined only where $|\nabla_a \Psi| > 0$. Setting

$$\mathbf{S} = (S_\phi, S_\xi) \equiv (r_a G_\xi, -r_a G_\phi), \quad (63)$$

we finally arrive⁸ at the following *visco-plastic* system in place of (61):

$$\nabla_a \cdot \mathbf{S} = -f, (\phi, \xi) \in (0, 1) \times (0, Z), \quad (64)$$

with constitutive relations:

$$\mathbf{S} = r_a \left[\frac{\chi(|\nabla_a \Psi|) + \tau_Y/H}{|\nabla_a \Psi|} \right] \nabla_a \Psi \iff |S| > \frac{r_a \tau_Y}{H}, \quad (65)$$

$$|\nabla_a \Psi| = 0 \iff |S| \leq \frac{r_a \tau_Y}{H}. \quad (66)$$

3.1. REMARKS:

1. The system (64–66) is analogous to a nonlinearly viscous, visco-plastic fluid flow along a rectangular duct, $(\phi, \xi) \in (0, 1) \times (0, Z)$. In this analogy, the function f plays the role of the pressure gradient, here spatially dependent through the fluid concentrations and the varying annular geometry. The vector \mathbf{S} plays the role of the dominant components of the deviatoric stress tensor. The *yield stress* also varies spatially, and is given by $r_a \tau_Y/H$. The purely viscous part of the *effective viscosity* is $r_a \chi(|\nabla_a \Psi|)/|\nabla_a \Psi|$. As $|\nabla_a \Psi| \rightarrow 0$, we have that $\chi(|\nabla_a \Psi|) \sim |\nabla_a \Psi|^{1/(m+1)}$. Thus, the purely viscous part, $r_a \chi(|\nabla_a \Psi|)/|\nabla_a \Psi| \rightarrow \infty$ as $|\nabla_a \Psi| \rightarrow 0$, but note that $\chi(|\nabla_a \Psi|) \rightarrow 0$. This is analogous locally to power-law behaviour, with index < 1 , *i.e.* shear-thinning.
2. Equation (64) is essentially a quasilinear elliptic equation for the stream function Ψ , (at least where $|\nabla_a \Psi| > 0$; see (61)). The formulation (64–66) can be regarded as the classical formulation of this problem, which results from the physical derivation presented. A more rigorous mathematical definition can be given as a variational inequality, which we believe will lead to rigorous existence and uniqueness results. This approach is currently being pursued. For the classical Bingham fluid problem, existence and uniqueness results are given in [39, pp. 278–326], [40, pp. 78–95] for a single fluid; for two fluids and for spatially dependent physical properties, further results can be found in [41–43]. The only technical difficulty appears to be with the nonlinear behaviour of the term $r_a \chi(|\nabla_a \Psi|)/|\nabla_a \Psi|$, and at 0. Here the methods of convex analysis (see *e.g.* [44]) appear to be applicable.
3. Apart from the analogy as a nonlinear visco-plastic duct flow, other analogies clearly exist. The most obvious one, via our derivation, is to note that the displacement flow is essentially a flow of multiple visco-plastic fluids in a long Hele-Shaw cell, that shows an *eccentric annular* variation in the gap thickness $H(\phi, \xi)$.
4. A further analogy is with the nonlinear seepage laws associated with the flow of non-Newtonian fluids in porous media. Certain heavy crude oils and even Newtonian fluids flowing through argillaceous rock can exhibit visco-plastic behaviour, insofar that there

is no flow unless a certain limiting pressure gradient is exceeded. Reservoir flows of this type have been studied extensively and effectively by Entov and co-workers, see [45], [46, pp. 44–51, 197–222].

3.2. BOUNDARY CONDITIONS

Boundary conditions are required for the system (64–66). On the wide side of the annulus, $\phi = 0$, we define the stream function to be zero:

$$\Psi(0, \xi, t) = 0. \quad (67)$$

Since the flow is incompressible, we have:

$$\Psi(1, \xi, t) = Q(t), \quad (68)$$

where the dimensional flow rate is $\hat{Q}(\hat{t}) = \hat{Q}^* Q(t)$. At the upper end of the annulus, we impose an outflow condition:

$$\frac{\partial \Psi}{\partial \xi}(\phi, Z, t) = 0. \quad (69)$$

At bottom-hole $\xi = 0$, the correct condition is less clear. At any one time a single fluid is being pumped into the annulus, turning around from its downwards descent inside the casing. Undoubtedly the flows are three-dimensional and complex locally. Fortunately, cemented annuli are long and we can expect three-dimensional effects to be confined to an entry length region at bottom-hole. Ignoring the entry region, we impose

$$\frac{\partial \Psi}{\partial \xi}(\phi, 0, t) = 0. \quad (70)$$

The physical basis of (70) is that there will be no axial gradient in Ψ in a region where the geometry and fluid concentration does not change with ξ , *i.e.* we interpret (70) as relating to the annulus just above the entry region. An alternative inflow condition would be to have a uniform inflow velocity imposed.

4. Results

Our final model consists of (64–66), the stream function definition (39) and the concentration equations (42), with associated geometric, boundary and initial data. As a base model for simulating the bulk features of cementing displacement flows, this suffices. For the most part, the fluids are advected through the annulus, (42). The fluid mixture will flow (or not) in any section according to the criterion (66), which corresponds physically to the underlying fluids having yielded or not, across the gap width. Thus, the model is clearly able to simulate an unyielded channel of mud remaining left behind on the narrow side of the annulus. However, the model remains fairly basic and we discuss some of the areas where improvements could be made in Section 5.

4.1. OUTLINE OF NUMERICAL ALGORITHM

In choosing a numerical algorithm, our prime concerns are of robustness and speed, rather than high accuracy. The intended usage of the model is for frequent re-runs of cementing

displacement simulations, *i.e.* iterating towards a near-optimal design. Considering (42) and (64), it is clear that some decoupling occurs, which can be exploited. Time dependency occurs only in the concentration equations. For given fluid concentrations at time t , the solution of (64) determines Ψ for a given flow rate $Q(t)$. This stream function Ψ then defines the velocity field through (39), which is used to advance the fluid concentrations in time via (42).

This problem structure leads naturally to a numerical algorithm in which (42) is solved explicitly on each timestep, from known values of the velocity field. For the solution of (42) we have used the flux-corrected-transport (FCT) scheme, [49]. Whilst more refined schemes are available, the FCT scheme has been found to be robust and gives acceptable accuracy for a practical computation. Shortcomings are discussed in Section 5.

To resolve (64) we have used a hybrid asymptotic-numerical method. The annulus is relatively long, $Z \sim 10^2 - 10^3$, and this prompts us to use a perturbation method for (64). We define $\epsilon = 1/Z$, rescale axial and azimuthal lengths and velocities in the usual fashion for *long-thin* problems, expand Ψ in a regular perturbation series: $\Psi \sim \Psi_0 + \epsilon\Psi_1 + \dots$, and substitute everything into (64). This leads to a sequence of one-dimensional boundary-value problems, to be solved on *slices* at fixed values of ξ , *i.e.* in place of (64). Our computation of Ψ comes from solving for the first two terms in this perturbation expansion, which satisfy (when yielded):

$$\frac{\partial}{\partial\phi} \left[\left(\frac{\chi(|\Psi_{0,\phi}|/r_a) + \tau_Y/H}{|\Psi_{0,\phi}|/r_a} \right) \frac{\partial\Psi_0}{\partial\phi} \right] = -\frac{r_a \cos\beta}{St^*} \frac{\partial\rho}{\partial\phi}, \quad (71)$$

$$\frac{\partial}{\partial\phi} \left[\chi'(|\Psi_{0,\phi}|/r_a) \frac{\partial\Psi_1}{\partial\phi} \right] = -\frac{r_a \sin\pi\phi}{St^*} \frac{\partial}{\partial z} [r_a \rho \sin\beta], \quad (72)$$

with boundary conditions

$$\Psi_0(0, z, t) = 0, \quad \Psi_0(1, z, t) = Q(t), \quad (73)$$

$$\Psi_1(0, z, t) = 0, \quad \Psi_1(1, z, t) = 0. \quad (74)$$

The derivation of this system is straightforward. To solve (71–74) numerically, both $[\chi(|\Psi_{0,\phi}|/r_a) + \tau_Y/H]/[|\Psi_{0,\phi}|/r_a]$ and $\chi'(|\Psi_{0,\phi}|/r_a)$ are regularized at 0, as has become common in visco-plastic fluid flow problems, (*i.e.* the viscosity does not become infinite, merely large). Solution of (71–74) is fast and very robust. Note that the speed of computation scales linearly with the number of gridpoints N used to discretise the annulus. This compares very well with conventional methods for solving the fully two-dimensional equation (64), typically between $N^{5/4}$ and N^2 . Additionally, solution of (71–74) can be *localized* to those depths at which the fluid concentrations change on each timestep, *i.e.* close to the interface. At other depths, unless the flow rate changes, Ψ does not vary with time. Obviously, some compromise is made in that the fully two-dimensional equation (64) is not solved.

4.2. NUMERICAL RESULTS

We present a number of illustrative results from our model. For the first three results, we consider cementing 1000m of casing, between depths 500m and 1500m in the well. Our azimuthal discretisation is 30 gridpoints and the axial discretisation is 100 gridpoints. For simplicity the mesh is uniform.

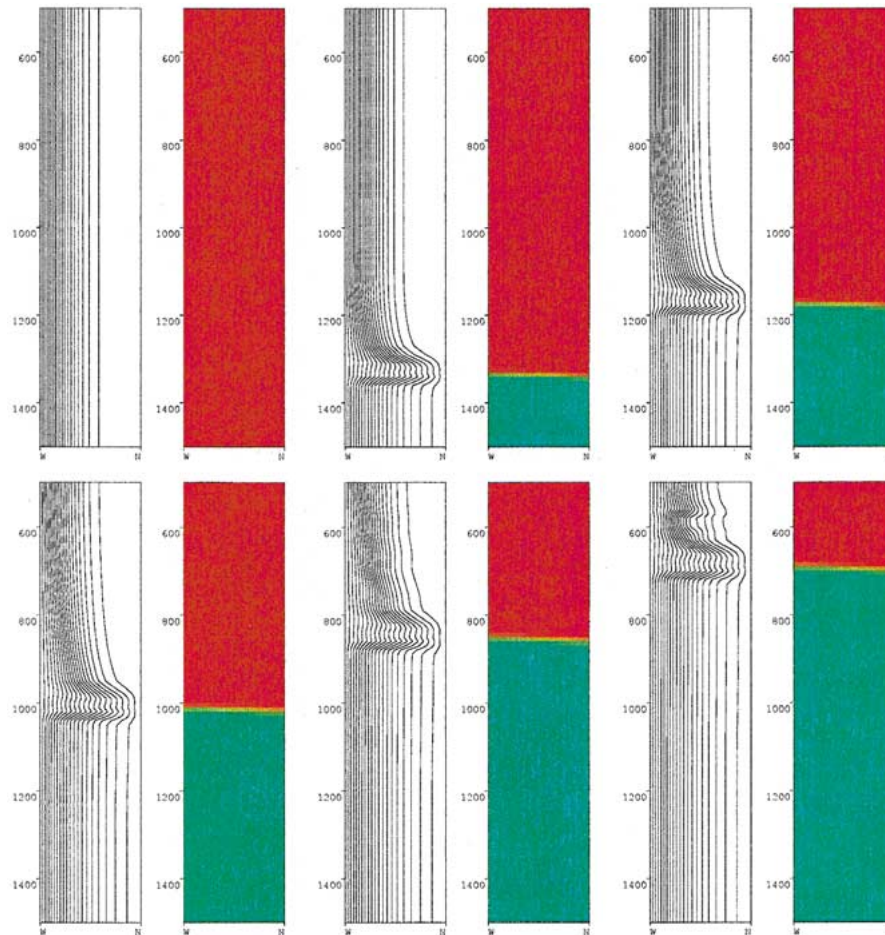


Figure 3. Results from simulating the displacement of example 1. Output at times $\hat{t} = 0, 200, 400, 600, 800, 1000$ seconds, after the spacer enters the annulus; (left to right, top to bottom). Each snapshot shows the fluid concentrations and the fluid streamlines; the latter spaced at contour intervals $\Delta\Psi = 0.05$. The wide ($\phi = 0$) and narrow ($\phi = 1$) sides of the annulus are denoted W and N, respectively.

4.2.1. Example 1: An eccentric annular displacement

An $8\frac{1}{2}$ in diameter casing (215.9mm) is to be cemented inside a uniform $9\frac{5}{8}$ in hole (244.475mm). The casing has 80% stand-off, (meaning $e(\xi) = 0.2$). The annulus is initially full of a 12ppg drilling mud ($=1440\text{kg/m}^3$), with rheological parameters: yield stress, $\hat{\tau}_{Y,1} = 10\text{lb/100ft}^2$, ($= 4.79\text{Pa}$), power law index, $n_1 = 0.7$, consistency, $\hat{k}_1 = 0.02\text{Pas}^{0.7}$. The mud is displaced by a spacer fluid with density 15ppg, ($\approx 1800\text{kg/m}^3$), and rheological parameters: $\hat{\tau}_{Y,2} = 15\text{lb/100ft}^2$, ($= 7.05\text{Pa}$), power law index $n_2 = 1.0$ and consistency $\hat{k}_2 = 0.03\text{Pas}$. A total of 30m^3 of spacer are pumped, at $0.5\text{m}^3/\text{min}$. The well is assumed vertical. Results are shown in Figure 3.

This situation is somewhat ideal. The well is vertical, the displacing fluid is more dense and viscous than the displaced fluid. Certainly, our intuition would be that the displacement will be effective. This intuition appears to be confirmed in Figure 4. The interface (*i.e.* concentration front) advances steadily up the wellbore. The front on the wide side of the annulus

is slightly in advance of that on the narrow side, but this gap does not appear to widen. The results suggest that we are seeing a stable steady-state displacement. This is not surprising. If for example, the annulus were vertical and concentric, we would certainly have a trivial steady-state displacement solution, namely a uniform horizontal interface. The stability of this solution would depend on the speed of displacement and the rheology of the two fluids. Classical analyses of the stability of this type of displacement front, *i.e.* in a porous media, are many; see [33–35].

Observe in Figure 3 that the streamlines are uniform and parallel both far upstream and downstream of the displacement front. Distortion of the streamlines occurs only close to the front. The steady state is signified by a uniform azimuthal distribution of streamlines. In a moving frame of reference, it appears that there would be two recirculatory zones, upstream and downstream of the front. It is noteworthy that the flow is countercurrent on either side of the steady state, *i.e.* the fluid flows from the wide to the narrow side in the displacing fluid and from the narrow to the wide side in the displaced fluid.

4.2.2. Example 2: A static mud channel

An $8\frac{1}{2}$ in diameter casing (215.9mm) is to be cemented inside a uniform $9\frac{5}{8}$ in hole (244.475mm). The casing has 50% stand-off, ($e(\xi) = 0.5$). The annulus is initially full of the same mud as in example 1. The mud is displaced by a spacer fluid with density 12ppg ($= 1440\text{kg/m}^3$), and rheological parameters: $\hat{\tau}_{Y,2} = 5\text{lb}/100\text{ft}^2$, ($= 2.35\text{Pa}$), power law index $n_2 = 1.0$ and consistency $\hat{\kappa}_2 = 0.01\text{Pas}$. A total of 30m^3 of spacer are pumped, at $0.5\text{m}^3/\text{min}$. The well is assumed vertical. Results are shown in Figure 4.

The situation here is similar to example 1, but now the viscosity and yield stress of the displacing fluid are below that of the drilling mud, the eccentricity is increased and there is no density difference. The spacer can be seen to move to the wide side of the annulus and channel upwards through the mud, leaving behind a static channel of mud on the narrow side of the annulus. This might be interpreted as a form of viscous fingering. We note that the mud moves more freely, on the narrow side of the annulus, in the part of the annulus ahead of the displacing fluid, *i.e.* if the mud were to be pumped on its own, a larger part of the annular area would be in contact with mobile mud than if pumped in parallel with this spacer fluid. Clearly, a displacement such as that in Figure 4 will result in a poorly cemented well.

4.2.3. Example 3: A more complex well

We now consider a more complex situation, characteristic of cementing operations. The hole diameter is mostly $9\frac{5}{8}$ in (244.475mm), but is non-uniform. There is an 11in (279.475mm) diameter washed-out section of the well, between 800m and 900m. The well builds slowly from being vertical at surface to being inclined 50 degrees from vertical at bottom hole. The stand-off is mostly at 80%, but drops to 50% between 1200m and 1300m. Fluid 1, the drilling mud, is as in examples 1 and 2. Fluid 2 is a spacer fluid with density 12ppg ($= 1440\text{kg/m}^3$), and rheological parameters: $\hat{\tau}_{Y,2} = 8\text{lb}/100\text{ft}^2$ ($= 3.76\text{Pa}$), power law index $n_2 = 1.0$ and consistency $\hat{\kappa}_2 = 0.01\text{Pas}$. Fluid 3 is a cement slurry, with density 15ppg ($= 1800\text{kg/m}^3$), and rheological parameters: $\hat{\tau}_{Y,3} = 15\text{lb}/100\text{ft}^2$ ($= 7.05\text{Pa}$), power law index $n_3 = 1.0$ and consistency $\hat{\kappa}_3 = 0.03\text{Pas}$. The flow rate is the same as in examples 1 and 2; 5m^3 of spacer is followed by 25m^3 of cement slurry. Results are shown in Figure 5.

The first frame shown in Figure 5, (top left), is just prior to the spacer entering the annulus. The two sections of the annulus, that where the well is most eccentric and that where the annulus is wider, are both clearly visible in the streamline pattern. In the washed out section,

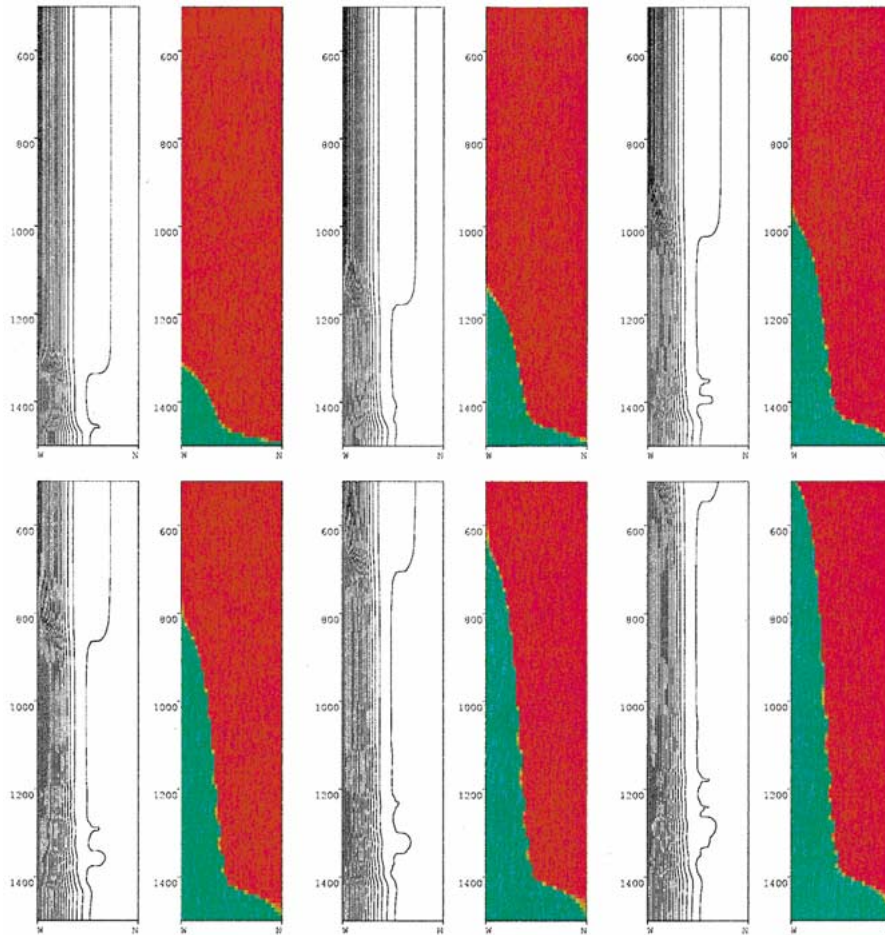


Figure 4. Results from simulating the displacement of example 2. Output at times $\hat{t} = 100, 200, 300, 400, 500, 600$ seconds, after the spacer enters the annulus; (left to right, top to bottom). Each snapshot shows the fluid concentrations and the fluid streamlines; the latter spaced at contour intervals $\Delta\Psi = 0.05$. The wide ($\phi = 0$) and narrow ($\phi = 1$) sides of the annulus are denoted W and N, respectively.

the pressure gradient drops and the region of slowly moving (or static) mud on the narrow side expands. As the spacer enters the annulus, it moves to the wide side, as in example 2, and bypasses the poorly centred part of the annulus on the wide side. The spacer, being less viscous than the mud, essentially fingers upwards on the wide side. As the cement enters the annulus, it displaces the spacer and mud at the bottom of the well. Displacement by the cement is much better than by the spacer, throughout the poorly centred section of the annulus, although it is still not complete. The slurry eventually displaces the other fluids from most of the annulus.

4.2.4. *Example 4: Near horizontal wells*

Finally, we consider cementing of a near horizontal well. Since the early 1990's, drilling of horizontal wells has become increasingly commonplace in the oil industry. The chief idea is to align the final section of the well with the reservoir, thus increasing production. The final section of the well may be left uncased, (an open-hole completion), or may be cemented and

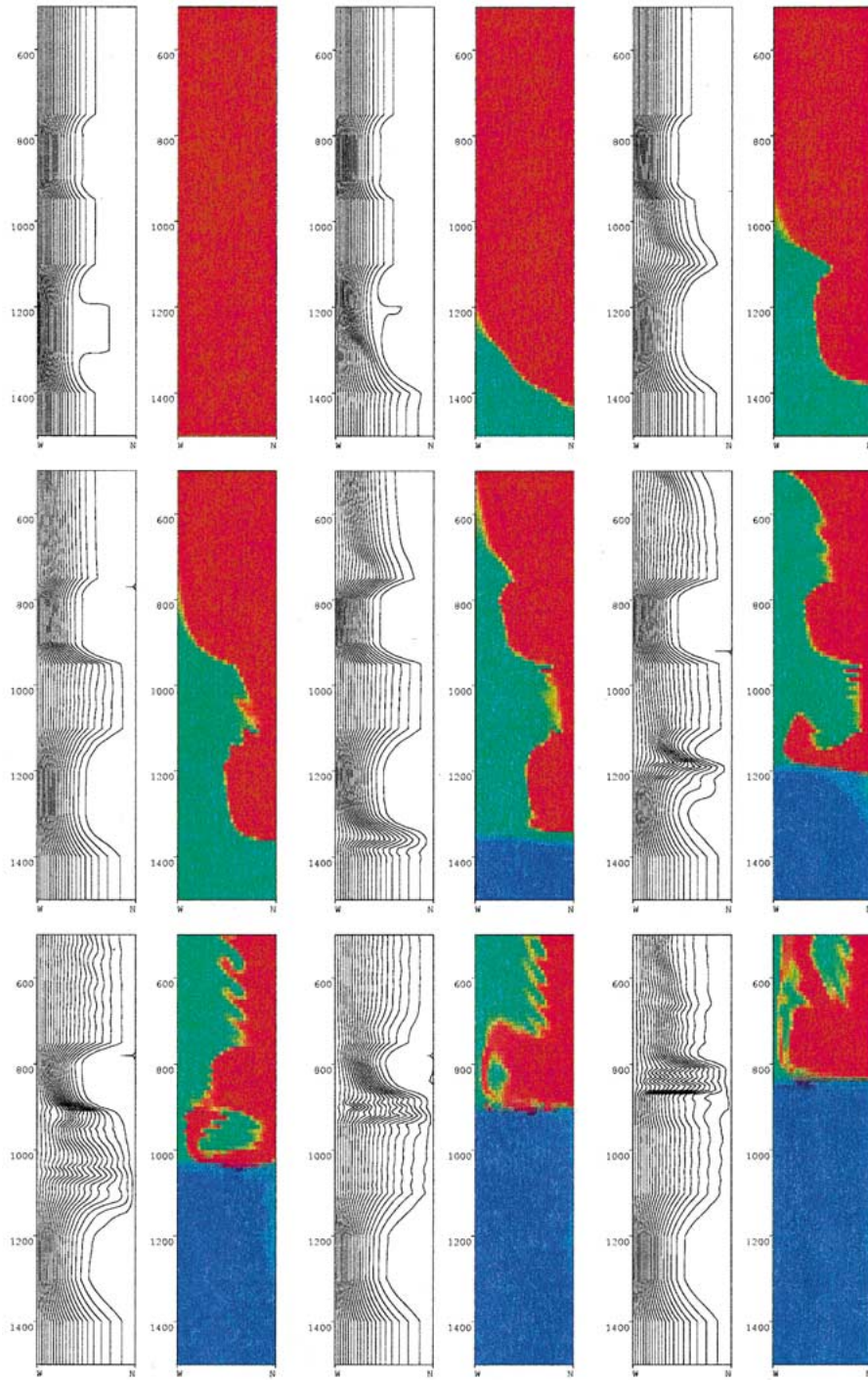


Figure 5. Results from simulating the displacement of example 3. Output at times $\hat{t} = 0, 200, 400, 600, 800, 1000, 1200, 1400, 1600$ seconds, after the spacer enters the annulus; (left to right, top to bottom). Each snapshot shows the fluid concentrations and the fluid streamlines; the latter spaced at contour intervals $\Delta\Psi = 0.05$. The wide ($\phi = 0$) and narrow ($\phi = 1$) sides of the annulus are denoted W and N, respectively.

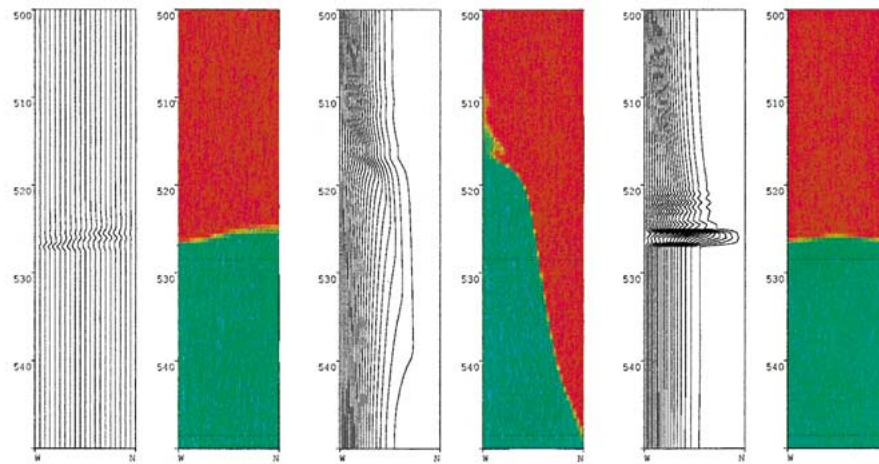


Figure 6. Results from simulating the displacement of example 4. Output at time $\hat{t} = 150$ seconds, after the spacer enters the annulus, for the different scenarios discussed. Each snapshot shows the fluid concentrations and the fluid streamlines; the latter spaced at contour intervals $\Delta\Psi = 0.05$. The wide ($\phi = 0$) and narrow ($\phi = 1$) sides of the annulus are denoted W and N, respectively.

then perforated. Regardless, the penultimate section is also near horizontal and this presents special problems for cementing displacements. As an example we consider a displacement along a very short 50m section, with a $8\frac{1}{2}$ in (215.9mm) diameter casing being cemented into a $9\frac{5}{8}$ in (244.475mm) hole, inclined at 85 degrees to the vertical. We suppose that the drilling mud is 10ppg ($\approx 1200\text{kg/m}^3$), with rheological parameters: yield stress, $\hat{\tau}_{Y,1} = 10\text{lb}_f/100\text{ft}^2$, ($= 4.79\text{Pa}$), power law index, $n_2 = 1.0$, consistency, $\hat{\kappa}_1 = 0.02\text{Pa}\cdot\text{s}$. The mud is displaced by a spacer fluid being pumped slowly, at $0.1\text{m}^3/\text{min}$. Our results are shown in Figure 6 for a variety of scenarios, each figure showing the situation 150 seconds after the spacer enters the annulus.

In Figure 6a we illustrate what happens when the annulus is perfectly concentric, ($e(\xi) = 0$), but the displacing fluid is heavier than the mud. We assume a spacer fluid with density 20ppg ($\approx 2400\text{kg/m}^3$), and rheological parameters: $\hat{\tau}_{Y,2} = 12\text{lb}_f/100\text{ft}^2$ ($= 5.64\text{Pa}$), power law index $n_2 = 1.0$ and consistency $\hat{\kappa}_2 = 0.03\text{Pa}\cdot\text{s}$. As might be expected, the heavier fluid slumps down towards the lower side of the annulus as it moves along the section. This effect is enhanced if the annulus is closer to horizontal, or if the density difference is increased, or if the flow rate is reduced.

In Figure 6b we show a displacement of the same mud by a spacer with the same rheological properties as for Figure 6a, but with density 10ppg ($\approx 1200\text{kg/m}^3$). The annulus is assumed to be eccentric ($e(\xi) = 0.3$), as is very common in near horizontal wells. A broad channel of static mud is left behind on the narrow side of the annulus, as in Section 4.2.2.

In Figure 6c we show that the gravity-driven slumping of Figure 6a can be used to reduce the extent of the mud channel in Figure 6b, *i.e.* the density difference can be used to force fluid around to the narrow side of the annulus. Here the spacer is as for Figure 6a, (density 20ppg), and the well is eccentric as for Figure 6b. The results are quite remarkable. Only a very narrow static channel remains behind on the narrow side of the annulus. The streamline plot shows clearly that close to the interface, the spacer is being forced down to the narrow side and the mud is moving upwards to the wide side.

Unfortunately, the results of Figure 6c are not easy to achieve, in the sense that quite a delicate balance is being observed. The general tendency when eccentric is for the interface to advance on the wide side as an extending finger. If this finger extends too far ahead, it can cease to be stable, since a lighter fluid lies underneath the finger in the azimuthal direction. In many cases the *viscous* finger will start to finger azimuthally under the action of gravity. These instabilities are observable in our model. However, it becomes hard to distinguish between physical and numerical phenomena after the onset of such instabilities; a *process model* is not the ideal medium for their study. Practically, where such instabilities occur in a near horizontal well, fluid mixing and contamination is likely to occur. Although the azimuthal flows may improve mud displacement in a volumetric sense, the end effect might not be a cemented well with effective zonal isolation.

It is noteworthy that while a number of technical papers exist that address issues in the cementing of horizontal wells, *e.g.* [13–15], none has succeeded to make any meaningful quantitative analysis. Horizontal well cementing is clearly an area with many fluid-engineering challenges still outstanding.

5. Discussion

In this paper we have derived a two-dimensional model of the displacement flows that occur in the primary cementing process. Although requiring numerical solution, certain features of the flows, *e.g.* steady-state displacements and static channels on the narrow side, may be amenable to further analysis. The third numerical example is illustrative primarily of the process complexity that must be accounted for in the design of a cementing job. Typically, variations in standoff and inclination occur all along the well, hole-diameter variations can occur due to drilling through weak or unconsolidated rock formations. The flow rate is not constant; a constant rate is imposed at the pumps, but U-tubing also can occur. A sequence of 3 to 4 rheologically different fluids being pumped is quite standard, followed by a drilling mud.

The above features can all be accounted for in a model of the type that we have presented, and this is a major strength of the model. However, inevitably there are also shortcomings. Probably the most important assumptions that we have made are: (i) that the fluids are homogeneous across the annulus gap; (ii) ignoring via scaling laws what happens very close to the interface; (iii) the simple mixture closure laws for the rheological constants. In certain situations each of these assumptions will break down. Effectively, our model is valid only when the fine-scale features of the displacement, close to the interface between the fluids, do not affect the bulk flow. However, the physical mechanisms underlying the fine scale features of the displacements studied here are far from fully understood.

A serious question is as to the robustness of our results for engineering purposes. A general statement here would be that the simulation results must be interpreted with some knowledge of the types of phenomena that can occur in a laminar displacement, in visco-plastic flows and with some consideration of potential numerical effects. For example, the simple mixture closure laws for the rheological constants stated in Section 2.2.1 are theoretically irrelevant, since (42) contains no diffusive term and intermediate concentrations are not specified in initial conditions. However, many numerical methods for (42) will exhibit numerical diffusion, so that intermediate concentrations are created and the mixing laws do become relevant. Thus, whereas in examples 1, 2 and 4 numerical diffusion is not excessive, in example 3 one might

question the effects of the mixing laws on the results. On the other hand, in example 3, the picture of most interest to a cementing engineer is the concentration at the end of the process. Although one might not believe the accuracy of the representation of the flow at intermediate times, an engineer observing Figure 5 is clearly alerted to the ineffectiveness of the spacer fluid and the likelihood of there remaining either contaminated cement or a mud channel on the narrow side of the annulus. The message is clear, that the cement job needs to be redesigned.

Results such as in example 1 and 2 are robust numerically and physically: small changes in the physical parameters still lead to a steady (and apparently stable) displacement in example 1, and to a static mud channel in example 2. It is interesting to note the fine scale features of the streamline towards the narrow side mud channel in Figure 4. Although one might think that this is a purely numerical effect, it is not believed to be so. The narrow side mud is unyielded, but only marginally so. Any small perturbation in the flow can cause the mud to yield locally and move. This type of marginal stability is quite common in visco-plastic flows. In certain situations, the flow can evolve in such a way that the yield surfaces at a particular point become stable (*i.e.* the local stresses decrease with time) and the yield surfaces are *frozen* or *foot-printed* into their position. Examples of this phenomena include [20, 47, 48]. Here, the yield surface remains marginally stable and there is no foot-printing. Although the cause of perturbation may be numerical error, the phenomena is physical and the flow is not unstable. Thus, in spite of the acknowledged limitations to our model, it is possible to make physically robust predictions that we expect to give at least qualitatively correct information, often more. Compared to rule-based systems for laminar displacements, [5–9], such models are a clear step forward.

There are also many primary cementing jobs that cannot be simulated by our model, as it stands. For example, many cementing jobs are pumped in turbulent regime, either fully or partially. It is also possible locally that the narrow side of the annulus is in laminar regime, but the wide side is turbulent. Modelling of this flow complexity offers many challenges. Another example concerns the practice of slowly rotating the casing as the job is pumped. This has the effect of shearing the annular fluids and reducing their viscosity. For single fluids in concentric annuli, known effects of shear thinning via rotation of one of the cylinders are summarised in [50]. This method is used in many industrial processes; see for example [51] for a recent application to food mixing. For a cementing flow, since both the displaced and displacing fluids are sheared, it is unclear what the net effect will be on the displacement, of slow rotation of the casing.

Although the above areas offer interesting challenges, our current directions for future research concern deeper understanding of the system (64–66), coupled with the concentration equations (42), and the development of more effective numerical solution algorithms. The shortcomings of our asymptotic-numerical method for (64) are firstly, that the fully two-dimensional equation (64) is not actually solved and secondly, that we need to regularize the constitutive relations (65) and (66). In ongoing work we are implementing an augmented Lagrangian algorithm that avoids both shortcomings and are also working on theoretical questions of existence and uniqueness of solutions to (64–66). In solving (42), our numerical examples show a certain amount of numerical diffusion at the interface between fluids. Although a front-tracking method could eliminate this problem, flows such as in our example of Section 4.2.3. would still be very challenging for such a method. We are encouraged by the continuing improvements in VOF methods, (as for example in [52]), and this might represent the best current method for improving the numerical solution of (42). Regarding experimental

validation, aside from [26, 27], an experimental eccentric annular displacement flow loop is under construction at University of British Columbia. We hope to report the results of experimental studies and the above mentioned analysis in the near future.

Acknowledgements

The management of Schlumberger are thanked for their permission to publish this paper. The contribution of IAF has been supported by Schlumberger and NSERC through CRD project 245434 and also by the Pacific Institute for the Mathematical Sciences. This support is gratefully acknowledged.

Notes

¹The effective circulating pressures must be high enough to prevent formation fluids from entering the bore-hole, but low enough not to fracture the surrounding formation.

²Compressibility is relevant in well construction flows, but only insofar that the static pressure in the well can be significantly affected.

³Certainly visco-elasticity can be important in certain situations and for certain wellbore fluids. Additionally, if static, a gel-strength generally builds up. When flowing, both drilling muds and cement slurries are predominantly shear thinning, nonlinearly viscous and inelastic, often with a significant yield stress. The phenomenon of a static layer of mud occupying the narrow side of the annulus following displacement is certainly attributable to the presence of a yield stress. Drilling mud, spacer fluid and cement slurry compositions are continuously changing as a result of both technological advances and commercial pressures. Inevitably, any rheological model will fail to characterise every flow behaviour of such complex fluids. Rheological models such as the Bingham model or power law model are frequently used to characterise these well construction fluids. Thus, our later choice of the Herschel-Bulkley model does incorporate the current industry practice, but is also partly pragmatic in accepting its eventual inadequacy for certain situations.

⁴The neglected inertial terms which appear at first order in (31) and (32) are in fact of size $\sim \text{Re}^* \delta^* / \pi$, where

$$\text{Re}^* = \frac{\hat{\rho}^* [\hat{w}^*]^2}{\hat{\tau}^*} = \frac{\hat{\rho}^* \hat{w}^* \hat{\tau}_a^* \delta^*}{\hat{\mu}^*}$$

is a global Reynolds number for the displacement. We note that the first-order terms that have been neglected in (30)–(32), include inertial terms, neglected shear stress terms, an additional gravitational term in (30), and terms which arise from the slow axial variation of the geometry. It would therefore be complex to derive a higher-order model.

⁵The first assumption will allow us to average the fluid properties across the gap width and is a reasonable assumption to make, far away from the actual displacement front. If the displacement is effective, we expect the region close to the displacement front to be well-defined and not to extend over more than a few azimuthal length-scales, *i.e.* much smaller than the length of the well. In this frontal region there are also other questionable features of our model, and the model is not really targeted at resolving small-scale features of the displacement flow. The second assumption is also reasonable when far from the displacement front, *i.e.* in regions where the flow is a single fluid annular flow. Use of *slot*-approximations for modelling these flows is quite commonplace in the oil and gas well construction flows, and is found to be reliable for narrow eccentric annuli; see [16].

⁶We note in passing that for fully turbulent flows with miscible fluids, $\hat{D}^* \sim 10^{-3} \text{m}^2 \text{s}^{-1}$, so that even here we might neglect diffusive effects in the axial direction, although not in the azimuthal direction.

⁷Note that our symmetric slot flow assumption implies that the shear stress is zero in at the center of the slot, as in any plane Poiseuille flow.

⁸Since $f = \nabla_a \cdot \mathbf{m}$, with \mathbf{m} defined by (62), it follows that:

$$\nabla_a \cdot [\mathbf{S} + \mathbf{m}] = 0.$$

Thus, the vector function $\mathbf{S} + \mathbf{m}$ is solenoidal and can be represented via a *stream function*. The relevant *stream function* in this case is of course the pressure p .

References

1. M.J. Economides, Implications of cementing on well performance. In: E. B. Nelson (ed.), *Well Cementing*. Schlumberger Educational Services (1990) Chapter 1.
2. B. Nichol, Choosing economic options for shut-in wells with a risk assessment approach. Presentation at: *Cost-effective Abandonment Solutions, Technology Information Session*, Calgary May 3, 2000. Meeting organised by PTAC (Petroleum Technology Alliance Canada).
3. E.B. Nelson, *Well Cementing*. Schlumberger Educational Services (1990).
4. R.H. McLean, C.W. Manry and W.W. Whitaker, Displacement mechanics in primary cementing. *Society of Petroleum Engineers* paper number SPE 1488 (1966).
5. A. Jamot, Deplacement de la boue par le latier de ciment dans l'espace annulaire tubage-paroi d'un puits. *Revue Assoc. Franc. Techn. Petr.* 224 (1974) 27–37.
6. C.F. Lockyear and A.P. Hibbert, Integrated primary cementing study defines key factors for field success. *J. Petr. Techn.* December (1989) 1320–1325.
7. C.F. Lockyear, D.F. Ryan and M.M. Gunningham, Cement channelling: how to predict and prevent. *Society of Petroleum Engineers* paper number SPE 19865 (1989).
8. D. Guillot, H. Hendriks, F. Callet and B. Vidick, Mud removal. In: E. B. Nelson (ed.), *Well Cementing*. Schlumberger Educational Services, (1990) Chapter 5.
9. M. Couturier, D. Guillot, H. Hendriks and F. Callet, Design rules and associated spacer properties for optimal mud removal in eccentric annuli. *Society of Petroleum Engineers* paper number SPE 21594 (1990).
10. S. Brady, P.P. Drecq, K.C. Baker and D.J. Guillot, Recent technological advances help solve cement placement problems in the Gulf of Mexico. *Society of Petroleum Engineers* paper IADC/SPE 23927 (1992).
11. D.F. Ryan, D.S. Kellingray and C.F. Lockyear, Improved cement placement on North Sea wells using a cement placement simulator. *Society of Petroleum Engineers* paper number SPE 24977 (1992).
12. V.C. Kelessidis, R. Rafferty, A. Merlo and R. Maglione, Simulator models U-tubing to improve primary cementing. *Oil and Gas J.* March 7th (1994) 72–80.
13. S.R. Keller, R.J. Crook, R.C. Haut and D.S. Kulakofsky, Deviated-wellbore cementing: Part 1 - problems. *J. Petr. Techn.* August (1987) 955–960.
14. R.J. Crook, S.R. Keller, and M.A. Wilson, Deviated wellbore cementing: Part 2 - solutions. *J. Petr. Techn.* August (1987) 961–966.
15. F.L. Sabins, Problems in cementing horizontal wells. *J. Petr. Techn.* April (1990) 398–400.
16. I.C. Walton and S.H. Bittleston, The axial flow of a Bingham plastic in a narrow eccentric annulus. *J. Fluid Mech.* 222 (1991) 39–60.
17. P. Szabo and O. Hassager, Flow of viscoplastic fluids in eccentric annular geometries. *J. Non-Newtonian Fluid Mech.* 45 (1992) 149–169.
18. P. Szabo and O. Hassager, Simulation of free surfaces in 3-D with the arbitrary Lagrange-Euler method. *Int. J. Num Methods in Eng.* 38 (1995) 717–734.
19. P. Szabo and O. Hassager, Displacement of one Newtonian fluid by another: density effects in axial annular flow. *Int. J. Multiphase Flow* 23 (1997) 113–129.
20. M. Allouche, I.A. Frigaard, and G. Sona, Static wall layers in the displacement of two visco-plastic fluids in a plane channel. *J. Fluid Mech.* 424 (2000) 243–277.
21. I.A. Frigaard, O. Scherzer and G. Sona, Uniqueness and non-uniqueness in the steady displacement of two viscoplastic fluids. *ZAMM* 81 (2001) 99–118.
22. C. Gabard-Cuoq, Etude de la stabilité de films liquides sur les parois d'une conduite verticale lors de l'écoulement de fluides miscibles non-newtoniens. *These de l'Universite Pierre et Marie Curie* (PhD thesis) Orsay, France (2001) 303pp.
23. I.A. Frigaard, M. Allouche and C. Gabard-Cuoq, Setting rheological targets for chemical solutions in mud removal and cement slurry design. *Society of Petroleum Engineers* paper number 64998 (2001).
24. B.W. van de Fliert and J.B. van den Berg, Displacement of a viscoplastic fluid in an inclined slot. In: J. Molenaar (ed.), *Proceedings of the Thirty-sixth European Study Group with Industry(ESGI 36)*. Eindhoven University of Technology: EUT-Report-00-WSK-01 ISSN 0167-9708 (2000) 55–62.
25. M. Martin, M. Latil and P. Vetter, Mud displacement by slurry during primary cementing jobs - predicting optimum conditions. *Society of Petroleum Engineers* paper number SPE 7590, (1978).
26. A. Tehrani, J. Ferguson and S.H. Bittleston, Laminar displacement in annuli: A combined experimental and theoretical study. *Society of Petroleum Engineers* paper number SPE 24569 (1992).

27. A. Tehrani, S.H. Bittleston and P.J.G. Long, Flow instabilities during annular displacement of one non-Newtonian fluid by another. *Experiments in Fluids* 14 (1993) 246–256.
28. P.G. Saffman and G.I. Taylor, The penetration of a finger into a porous medium in a Hele-Shaw cell containing a more viscous liquid. *Proc. R. Soc. London A* 245 (1958) 312–329.
29. P.G. Saffman, Viscous fingering in Hele-Shaw cells. *J. Fluid Mech.* 173 (1986) 73–94.
30. G.M. Homsy, Viscous fingering in porous media. *Ann. Rev. Fluid Mech.* 19 (1987) 271–311.
31. G. Daccord, J. Nittman and H.E. Stanley, Radial viscous fingers and diffusion limited aggregation: fractal dimension and growth sites. *Phys. Rev. Lett.* 56 (1986) 336–339.
32. P. Coussot, Saffman-Taylor instability in yield-stress fluids. *J. Fluid Mech.* 380 (1999) 363–376.
33. H. Pascal, Rheological behaviour effect of non-Newtonian fluids on dynamic of moving interface in porous media. *Int. J. Engng. Sci.* 22 (1984) 227–241.
34. H. Pascal, Dynamics of moving interface in porous media for power law fluids with a yield stress. *Int. J. Engng. Sci.* 22 (1984) 577–590.
35. H. Pascal, A theoretical analysis of stability of a moving interface in a porous medium for Bingham displacing fluids and its application in oil displacement mechanism. *Can. J. Chem. Engng.* 64 (1986) 375–379.
36. Y.C. Yortsos and M. Zeybek, Dispersion driven instability in miscible displacement in porous media. *Phys. Fluids.* 31 (1988) 3511–3518.
37. Z. Yang and Y.C. Yortsos, Asymptotic solutions of miscible displacements in geometries of large aspect ratio. *Phys. Fluids.* 9 (1997) 286–298.
38. M. Mineev-Weinstein, Selection of the Saffman-Taylor finger width in the absence of surface tension: an exact result. *Phys. Rev. Lett.* 80 (1998) 2113–2116.
39. G. Duvaut and J.L. Lions, *Inequalities in Mechanics and Physics*. Heidelberg: Springer (1976) 397 pp.
40. R. Glowinski, *Numerical Methods for Nonlinear Variational Problems*. Heidelberg: Springer-Verlag (1984) 493 pp.
41. I.A. Frigaard and O. Scherzer, Uniaxial exchange flows of two Bingham fluids in a cylindrical duct. *IMA J. Appl. Math.* 61 (1998) 237–266.
42. I.A. Frigaard and J. Crawshaw, Preventing buoyancy-driven flows of two Bingham fluids in a closed pipe - Fluid rheology design for oilfield plug cementing. *J. Eng. Math.* 36 (1999) 327–348.
43. I.A. Frigaard and O. Scherzer, The effects of yield stress variation on uniaxial exchange flows of two Bingham fluids in a pipe. *SIAM J. Appl. Math.* 60 (2000) 1950–1976.
44. I. Ekeland and R. Temam, *Convex Analysis and Variational Problems*. North-Holland: Amsterdam (1976) 402pp.
45. R.V. Goldstein and V.M. Entov, *Qualitative Methods in Continuum Mechanics* (1989) 279pp.
46. G.I. Barenblatt, V.M. Entov, and V.M. Ryzhik, Theory of fluid flows through natural rocks. *Theory and Applications of Transport in Porous Media* volume 3 Kluwer (1990) 395pp.
47. K.F. Liu and C.C. Mei, Roll waves on a layer of muddy fluid flowing down a gentle slope - a Bingham model. *Phys. Fluids* 6 (1994) 2577–2590.
48. R.V. Craster and O.K. Matar, Surfactant transport on mucus films. *J. Fluid Mech.* 425 (2000) 235–258.
49. S.T. Salesak, Fully multi-dimensional flux-corrected transport. *J. Comp. Phys.* 31 (1979) 355–362.
50. R.B. Bird, R.C. Armstrong and O. Hassager, *Dynamics of Polymeric Liquids, Vol. 1, Fluid Mechanics*. (2nd ed.) New York: Wiley (1987).
51. A.D. Fitt and C.P. Please, Asymptotic analysis of the flow of shear-thinning foodstuffs in annular scraped heat exchangers. *J. Eng. Math.* 39 (2001) 345–366.
52. J. Li and Y. Renardy, Numerical study of flows of two immiscible liquids at low Reynolds number. *SIAM Rev.* 42 (2000) 417–439.